JOURNAL OF PETROLOGY | VOLUME 45 | NUMBER 12 | PAGES 2407–2422 | 2004 | doi:10.1093/petrology/egh057

High-pressure Partial Melting of Mafic Lithologies in the Mantle

T. KOGISO[1]*, M. M. HIRSCHMANN[2] AND M. PERTERMANN[3,4]

[1]INSTITUTE FOR RESEARCH ON EARTH EVOLUTION (IFREE), JAPAN AGENCY FOR MARINE–EARTH SCIENCE AND TECHNOLOGY (JAMSTEC), YOKOSUKA 237-0061, JAPAN

[2]DEPARTMENT OF GEOLOGY AND GEOPHYSICS, UNIVERSITY OF MINNESOTA, MINNEAPOLIS, MN 55455, USA

[3]INSTITUT FÜR MINERALOGIE UND PETROGRAPHIE, EIDGENÖSSISCHE TECHNISCHE HOCHSCHULE, CH-8902 ZÜRICH, SWITZERLAND

[4]PRESENT ADDRESS: DEPARTMENT OF GEOLOGY, UNIVERSITY OF ILLINOIS AT URBANA–CHAMPAIGN, URBANA, IL 61801, USA

RECEIVED SEPTEMBER 24, 2003; ACCEPTED JULY 2, 2004
ADVANCE ACCESS PUBLICATION SEPTEMBER 9, 2004

We review experimental phase equilibria associated with partial melting of mafic lithologies (pyroxenites) at high pressures to reveal systematic relationships between bulk compositions of pyroxenite and their melting relations. An important aspect of pyroxenite phase equilibria is the existence of the garnet–pyroxene thermal divide, defined by the enstatite–Ca-Tschermaks pyroxene–diopside plane in CaO–MgO–Al_2O_3–SiO_2 projections. This divide appears at pressures above ~2 GPa in the natural system where garnet and pyroxenes are the principal residual phases in pyroxenites. Bulk compositions that reside on either side of the divide have distinct phase assemblages from subsolidus to liquidus and produce distinct types of partial melt ranging from strongly nepheline-normative to quartz-normative compositions. Solidus and liquidus locations are little affected by the location of natural pyroxenite compositions relative to the thermal divide and are instead controlled chiefly by bulk alkali contents and Mg-numbers. Changes in phase volumes of residual minerals also influence partial melt compositions. If olivine is absent during partial melting, expansion of the phase volume of garnet relative to clinopyroxene with increasing pressure produces liquids with high Ca/Al and low MgO compared with garnet peridotite-derived partial melts.

KEY WORDS: *experimental petrology; mantle heterogeneity; partial melting; phase equilibrium; pyroxenite*

INTRODUCTION

Partial melting of mantle material in the Earth's interior is one of the essential processes responsible for the thermal and chemical evolution of the Earth. Partial melting of peridotite, the predominant lithology in the upper mantle (e.g. Ringwood, 1975; McDonough & Sun, 1995), is thought to be responsible for the genesis of various types of mafic magmas, such as mid-ocean ridge basalts (MORB), ocean island basalts (OIB), and volcanic arc basalts (e.g. McKenzie & Bickle, 1988). During recent decades, there have been a number of experimental studies on partial melting of peridotite (e.g. Jaques & Green, 1980; Takahashi & Kushiro, 1983; Falloon & Green, 1988; Hirose & Kushiro, 1993; Baker & Stolper, 1994; Zhang & Herzberg, 1994; Walter, 1998). These experiments provide the foundation for quantitative understanding of the melting behavior of a homogeneous mantle (e.g. Klein & Langmuir, 1987; McKenzie & Bickle, 1988).

On the other hand, several lines of evidence indicate that the mantle contains a significant fraction of mafic lithologies (e.g. Schulze, 1989; Hirschmann & Stolper, 1996), which are olivine-poor relative to typical peridotite, and these may play an important role in basalt generation. Pyroxenite is a minor but ubiquitous lithology in virtually all natural mantle samples, including xenoliths and tectonically exposed mantle sections (Hirschmann & Stolper, 1996). On a larger scale, huge volumes of mafic rock produced by the continuing differentiation of the Earth have been returned to the mantle by subduction and other processes, and some of this material is believed to contribute to modern oceanic magmatism (e.g. Chase, 1981; Hofmann & White, 1982; Hofmann, 1997; Helffrich & Wood, 2001). A link

*Corresponding author. Present address: Department of Earth and Planetary Sciences, Tokyo Institute of Technology, Meguro, Tokyo 152-8551, Japan. Telephone: +81-3-5734-2338. Fax: +81-3-5734-3538. E-mail: kogisot@jamstec.go.jp

between recycled components and OIB geochemistry is well established, and variations in Sr–Nd–Pb–Os isotope compositions of OIB and their correlations with major elements suggest that at least in some cases the recycled geochemical signatures are delivered to basalt source regions by mafic lithological domains (e.g. Hauri, 1996; Kogiso *et al.*, 1997). Heterogeneity in major elements may also be attributed partly to partial melting of pyroxenitic rocks in the MORB source (le Roux *et al.*, 2002). On the other hand, the significance of pyroxenitic rocks in basalt source regions remains controversial and geochemical evidence has been used to argue both for and against an essential role for pyroxenite in various localities (Stracke *et al.*, 1999; Rudnick *et al.*, 2000; Salters & Dick, 2002; Michael *et al.*, 2003; Niu & O'Hara, 2003).

The study of pyroxenite lithologies in basalt source regions has two goals: allowing linkages between the compositions of oceanic basalts and the origin of mantle heterogeneities, and understanding the influence of pyroxenite on the chemistry and dynamics of melt generation. Addressing both questions requires experimental determination of melting relations of pyroxenite of appropriate compositions. However, as detailed in the following section, the range of pyroxenite compositions that could be present in basalt source regions is rather large. In this study, we review experimental phase equilibria associated with pyroxenite partial melting so as to gain an overview of the relationship between bulk composition and melting relations and of the effect of bulk composition on partial melt compositions.

VARIATIONS OF PYROXENITE COMPOSITION

In this study we focus on lithologies that we term 'pyroxenite', by which we mean rocks that are dominated by pyroxene under upper-mantle conditions. Unfortunately, the nomenclature for such rocks is not well established, and consequently, 'pyroxenite' serves as a catch-all for pyroxene-rich lithologies ranging from eclogites to olivine- and orthopyroxene-bearing rocks (websterites and olivine websterites) that lack sufficient olivine (40%) to be considered peridotitic. If considered as liquids, many of the bulk compositions of pyroxenite are broadly basaltic, with more MgO-rich varieties similar to picrites or basaltic komatiites. Some pyroxenites, such as olivine websterites and clinopyroxenites, may have no analogous naturally occurring lava types. These may originate as cumulates, as residues of partial melting, or by solid–solid or solid–melt hybridization processes.

The potential diversity of compositions of putative pyroxenites in basalt source regions is a significant hurdle to understanding their partial melting behaviors. Three approaches, which we term 'analogue', 'forward' and 'inverse', may yield some useful constraints for characterizing the diversity of pyroxenite in basalt source regions, each with its own advantages and disadvantages. In the analogue approach, compositions of mantle pyroxenites are surveyed from natural mantle samples, such as xenoliths and layers or pods in tectonically exhumed alpine-type massifs, ophiolites, and abyssal peridotites. The forward method considers likely compositions of pyroxenites based on models of mantle pyroxenite formation and modification. In the inverse approach, major element compositions of pyroxenite partial melts are extracted from correlations with a component thought to be indicative of a pyroxenitic source on the basis of isotopic or trace element signatures. Information about the composition of the pyroxenites themselves can then be inferred, provided sufficient information is available about the relationship between source rock and partial melt compositions.

The analogue approach is based on sampling of natural pyroxenite lithologies. Figure 1 shows oxide contents of pyroxenites from xenoliths and alpine-type massifs (Hirschmann & Stolper, 1996). They span compositions from near-peridotitic to basaltic (Fig. 1), with SiO_2 ranging from 40 to 55 wt %, MgO from 4 to 35 wt %, and Mg-number [$= 100 \times$ molar MgO/(MgO + FeO*)] from nearly 40 to over 90. This survey demonstrates that there could be many different compositions of pyroxenite residing in basalt source regions. However, it remains to be established whether such compositions are representative of those in principal basalt source regions. Importantly, most of the samples compiled in Fig. 1 come from the lithosphere rather than the convecting mantle, which is the predominant source of basaltic magmas. Samples from the lithosphere may not be representative of those from the convecting mantle. For example, certain types of pyroxenite, such as the clinopyroxenites common in ophiolite sections, may originate as veins in the lithosphere (e.g. Kelemen *et al.*, 1997) and consequently may not be appropriate analogues to mafic domains possibly present in mantle experiencing partial melting by decompression. However, such compositions can be introduced into the deeper mantle when regions of lithosphere are subducted or delaminated. Other pyroxenites may be modified by lithospheric processes such as metasomatism or partial melting at low pressures and therefore may not retain compositions indicative of the convecting mantle. Finally, transport to the surface, either by tectonic or volcanic processes, may result in compositional changes. We note that analogue approaches to defining compositions of mantle peridotite may be biased for similar reasons—most samples have experienced melting, metasomatic, and/or contamination in the lithosphere.

The forward approach to estimating compositions of pyroxenite in basalt source regions entails modeling

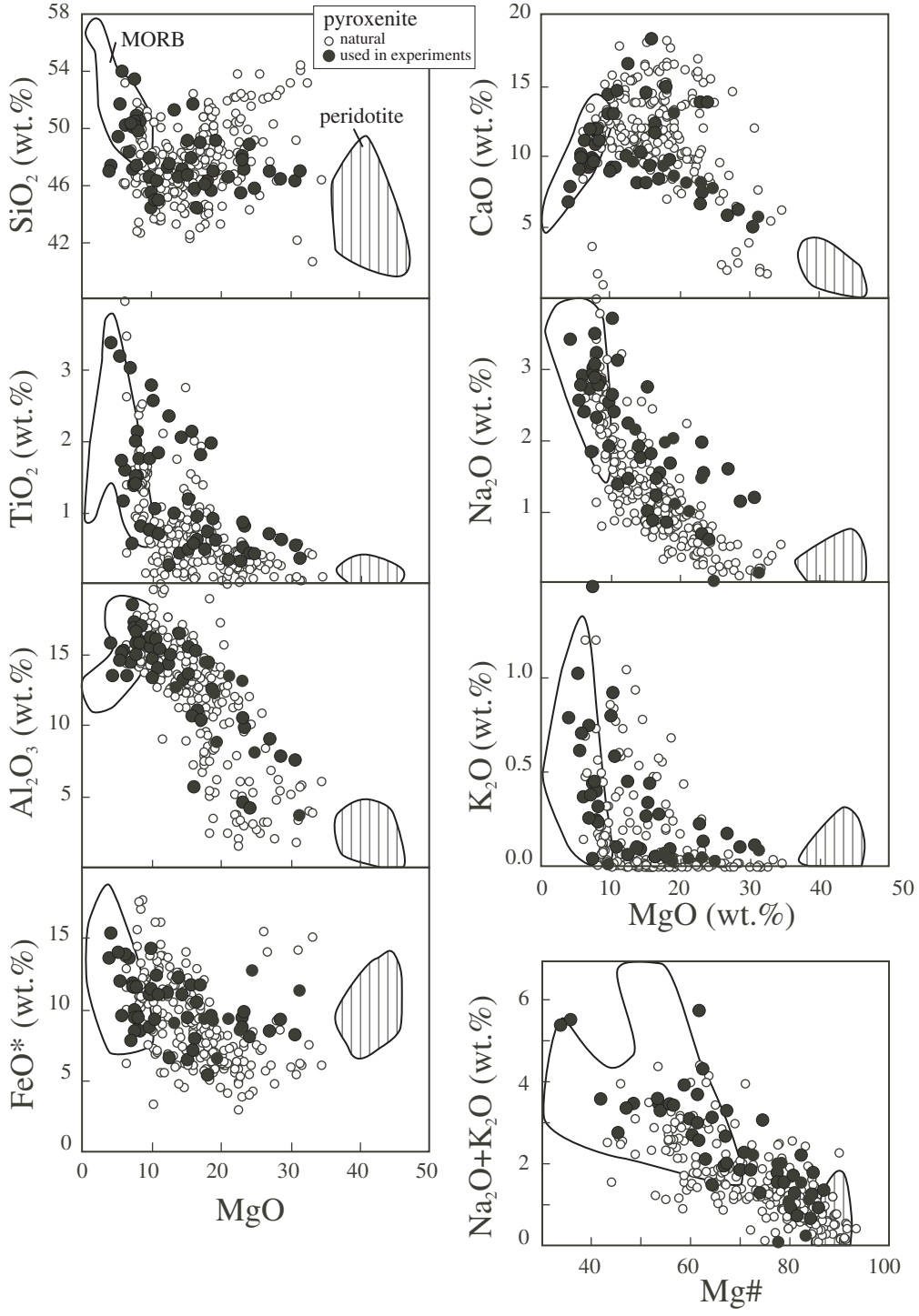

Fig. 1. Oxide contents of pyroxenite from xenoliths and alpine-type massifs (○) (Hirschmann & Stolper, 1996) and from experimental studies (●) (Table 1). Also shown are fields of mantle peridotite (Herzberg *et al.*, 1988) and MORB matrix glasses (Melson *et al.*, 1999).

processes that may introduce pyroxene-rich lithologies into the convecting mantle and considering the compositional changes that may occur prior to entering basalt source regions. Subduction may produce the largest volume of such lithologies but other processes, such as delamination of lower crust (e.g. Arndt & Goldstein, 1989; Jull & Kelemen, 2001) may be important. Various other possible sources of pyroxenite have been reviewed

previously by Hirschmann & Stolper (1996). We note that a popular paradigm for introducing heterogeneities into the mantle—metasomatism of oceanic lithosphere by near-axis melts from the MORB source region (e.g. Halliday *et al.*, 1995; Class & Goldstein, 1997; Niu & O'Hara, 2003)—probably results in veining, which means that such heterogeneous domains probably include some form of pyroxenite.

The composition of subducted oceanic crust is usually considered to be that of modern MORB that has been modified by alteration on the sea floor and by mass transport processes in subduction zones. However, it is important to note that most of the ~7 km section of modern oceanic crust consists of gabbro rather than basalt and that oceanic gabbro compositions are more varied than those of MORB (e.g. Dick *et al.*, 1991; Hekinian *et al.*, 1993). Also, significant sea-floor alteration and hydration may be restricted to the upper few kilometers of oceanic crust and reduced hydration of the lower portions of subducted crust may also mean less profound mass transport during sea-floor metamorphism and subduction. Finally, recycled lithologies present in the sources of modern basalts may have been subducted several billion years ago, when compositions of oceanic crust and subduction zone processes may have differed from those prevailing today (Komiya *et al.*, 2002*a*, 2002*b*).

The inverse approach is the least-developed method for determining the compositions of pyroxenite in basalt source regions. In a well-known example, Hauri (1996) considered the origin of silica enrichments associated with isotopic anomalies in the so-called Koolau component in Hawaii, which he inferred to originate from a dacitic partial melt. This in turn implies the presence of a quartz eclogite component in the source. Interestingly, the melt composition inferred by Hauri (1996) is not similar to any experimentally derived partial melt of eclogite (Pertermann & Hirschmann, 2003*a*). One possible reason for this is that pyroxenite partial melts may be modified by interactions with peridotite (Yaxley & Green, 1998; Takahashi & Nakajima, 2002) prior to contributing their components to aggregating basalts. This may be a significant pitfall of the inverse approach, but in tandem with appropriate experimental studies it could also lead to improved understanding of melt–rock interactions during melting and melt transport of a heterogeneous mantle.

Despite wide variations in pyroxenite composition, significant generalization can be made about bulk composition effects on partial melting behavior. Pyroxenites can be divided into two broad classes, silica-excess and silica-deficient, that produce distinctive compositions of partial melts. The chief differences between silica-excess and silica-deficient compositions are illustrated in Fig. 2, which shows normative compositions of pyroxenite plotted in the pseudoternary system forsterite (Fo)–Ca-Tschermaks pyroxene (CaTs)–quartz (Qz) projected from diopside [Di] (O'Hara, 1968). It should be noted that pyroxenite compositions are scattered over both sides of the enstatite (En)–CaTs join (Fig. 2). This join is a thermal divide (O'Hara & Yoder, 1967; O'Hara, 1968), which is stable when garnet and pyroxenes are principal minerals in the residue, as all stoichiometric garnet and pyroxene project along the En–CaTs join. Silica-deficient and silica-excess pyroxenites plot on the left and right side of the thermal divide, respectively. When garnet and pyroxenes are the chief minerals present, as is the case for most pyroxenite compositions above ~2 GPa (Table 1, see below), silica-deficient pyroxenites generate silica-poor melts that also plot on the left side of the divide, and silica-excess pyroxenites generate silica-rich melts that plot on the right side of the divide. The Fo–CaTs–Qz projection also indicates that pyroxenites of each type have characteristic accessory minerals: quartz (or its high-pressure equivalent), feldspar and/or kyanite for silica-excess pyroxenites and olivine and/or spinel for silica-deficient varieties (see inset of Fig. 2).

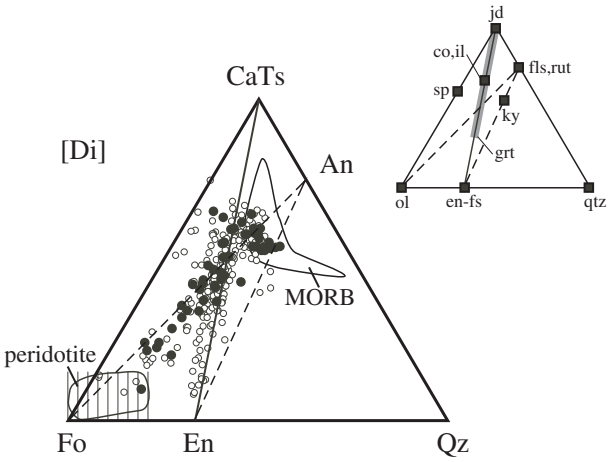

Fig. 2. Normative compositions of pyroxenite in the pseudoternary system forsterite (Fo)–Ca-Tschermaks pyroxene (CaTs)–quartz (Qz) projected from diopside [Di] using the method of O'Hara (1968). Symbols and fields are as in Fig. 1. Compositions of minerals are also shown in the inset. co, corundum; en-fs, enstatite–ferrosilite; fls, feldspar; grt, garnet; il, ilmenite; ky, kyanite; jd, jadeite; ol, olivine; rut, rutile; sp, spinel.

The garnet–pyroxene thermal divide is applicable to partial melting of pyroxenite in basalt source regions because garnet is stable in pyroxenite compositions over much of the pressure range relevant to present-day basalt genesis in the upwelling mantle (~1–4 GPa for MORB and OIB, McKenzie & Bickle, 1988; McKenzie & O'Nions, 1991; Iwamori *et al.*, 1995). Therefore, we mainly focus on melting relationships of pyroxenite at conditions under which garnet is stable. Details of phase equilibria and compositions of partial melts will be discussed in the following sections.

Table 1: Compositions of starting materials used in experimental studies of pyroxenite partial melting

Reference	Purpose of experiment[1]	Starting material	*P* (GPa)[2]	SiO_2	TiO_2	Al_2O_3	FeO*	MnO	MgO	CaO	Na_2O	K_2O	Cr_2O_3	P_2O_5	Total	Mg-no.	grt + cpx limit[3]
Yoder & Tilley (1962)	sol, liq	35090	0—3·14	50·05	1·55	13·37	13·73	0·25	6·49	11·00	2·38	0·36		0·12	99·30	45·7	1·0—2·0
Cohen *et al.* (1967)	sol, liq	NM5	0—4·98	49·93	1·34	16·75	11·40	0·18	7·59	9·33	2·92	0·37		0·19	100·00	54·3	1·6—1·9
Green & Ringwood (1967)	liq	ol basalt	0·9—2·7	47·05	2·31	14·17	11·02	0·16	12·73	9·87	2·21	0·44			99·96	67·3	1·35—1·8
		ol tholeiite	0—2·7	46·95	2·02	13·10	10·99	0·15	14·55	10·16	1·73	0·08		0·21	99·94	70·2	1·35—1·8
		alkali ol basalt	0—2·7	45·39	2·52	14·69	14·10	0·18	10·37	9·14	2·62	0·78		0·02	99·81	56·7	0·9—1·8
		picrite	1·35—2·7	45·51	1·93	12·44	9·50	0·15	18·79	9·67	1·64	0·08		0·20	99·91	77·9	
Kornprobst (1970)	sol, liq	M7-58	1·5—3·0	44·26	0·58	10·91	10·36	0·15	16·75	12·15	1·19	0·04	0·19	0·10	96·68	74·2	1·5—2·0
		M5-43	1·5—2·5	44·82	0·67	15·38	10·99	0·20	11·31	14·41	1·34	0·09	0·25	0·10	99·56	64·7	1·5—2·0
Irving (1974)	sol	R392	0·45—2·7	46·60	0·45	15·50	6·30	0·15	15·40	14·30	0·96	0·26	0·16	0·04	100·12	81·3	
		R394	0·81—2·25	46·10	0·70	14·40	5·30	0·16	18·40	14·80	0·82	0·04	0·05	0·03	100·80	86·1	
		R130	1·26—2·25	47·20	2·10	15·70	11·50	0·19	8·20	11·60	3·20	0·24	0·01	0·43	100·37	56·0	
		R698	0·5—1·5	50·30	0·78	16·90	8·40	0·18	8·60	11·00	2·80	0·31	0·02	0·08	99·37	64·6	
Ito & Kennedy (1974)	sol, liq, melt	eclogite	0—3·05	46·46	0·40	16·43	12·10	0·33	14·20	7·98	1·89	0·09			99·88	67·7	1·11—1·39
Thompson (1974)	liq, melt	SK931	1·0—2·2	46·86	3·34	15·68	13·55	0·20	4·31	6·66	4·75	0·77		0·47	96·59	36·2	2·2<
		SK971	0·5—2·5	46·94	1·37	17·15	11·73	0·19	7·69	9·73	3·01	0·43		0·18	98·42	53·9	1·8—2·0
		66108	0·8—3·1	46·12	1·81	13·94	12·22	0·18	11·08	9·05	3·11	0·57		0·23	98·31	61·8	1·9—2·0
Arculus (1975)	liq	AJI2164	1·0—3·0	44·19	2·75	13·26	11·33	0·18	10·30	8·77	3·71	2·02	0·03	0·97	97·51	61·8	2·5—2·7
		G531	1·0—3·5	44·78	1·02	15·95	9·13	0·18	10·71	12·81	2·38	0·91	0·03	0·37	98·27	67·6	2·5—3·0
Thompson (1975)	sol, liq, melt	OB32	0·5—3·5	47·17	4·15	13·34	15·22	0·23	4·42	7·68	3·40	2·00		1·39	99·00	34·1	2·2—2·5
		59-P-13	0·5—3·55	48·21	2·99	14·38	13·55	0·21	7·18	9·15	2·70	0·73		0·56	99·66	48·6	1·8—2·0
Obata & Dickey (1976)	sol, liq	R127	0·5—3·0	47·73	0·73	16·16	8·69	0·15	9·88	14·15	1·89	0·01	0·00	0·00	99·39	67·0	2·0—2·5
Kornprobst (1977)	sol	70-385B	3·0	49·00	0·60	8·63	6·57	0·15	19·4	13·08	1·10		0·32		98·85	84·0	
Johnston (1986)	liq, melt	SSS1·4	0·95—3·1	50·26	0·54	18·46	7·61	0·21	7·32	11·81	1·80	0·25			98·26	63·2	2·0—2·45
Wei *et al.* (1990)	sol, liq	M620	4·0—12·0	45·60	0·40	7·95	12·66	0·20	25·00	7·60	0·01	0·02			99·44	77·9	
		HSS-15	4·0—12·0	46·77	0·33	3·42	11·26	0·19	31·51	5·67	0·12	0·08			99·35	83·3	
Adam *et al.* (1992)	sol	DR9734	0·75—2·0	47·30	0·24	14·95	6·52	0·14	12·83	16·44	1·44	0·05	0·09		100·00	77·8	
Eggins (1992*a*)	liq	Kilauea tholeiite	1·0—3·5	47·76	2·09	10·53	11·61	0·15	15·98	9·26	1·79	0·43	0·13	0·20	99·93	71·0	2·0—2·5
Kinzler & Grove (1992)	melt	70-002 + 20% opx	0·9	51·14	0·97	12·66	9·08	0·14	13·63	9·57	2·14	0·08		0·10	99·50	72·8	
		79-35 g + 20% ol	1·3—1·6	45·98	0·47	14·40	9·30	0·14	17·94	9·28	1·94	0·07	0·03	0·02	99·58	77·5	
		SYN1	1·2	46·50	0·30	13·40	9·40	0·04	21·30	8·04	0·99	0·04	0·03		100·04	80·2	
		2004-3-1 + 25% ol	1·6	46·80	0·89	12·23	9·29	0·07	19·07	8·78	2·00	0·03		0·03	99·17	78·5	
Yasuda *et al.* (1994)	sol, liq, melt	NAM-7	3·0—20·0	49·71	1·71	15·68	9·37	0·18	8·43	11·73	2·76	0·23		0·02	99·82	61·6	

Table 1: continued

Reference	Purpose of experiment[1]	Starting material	P (GPa)[2]	SiO_2	TiO_2	Al_2O_3	FeO*	MnO	MgO	CaO	Na_2O	K_2O	Cr_2O_3	P_2O_5	Total	Mg-no.	grt + cpx limit[3]
Kinzler (1997)	melt	PMF1	1·7—1·9	45·40	0·29	13·00	8·83	0·03	23·20	7·97	1·47	0·04	0·00	0·06	100·29	82·4	
Takahashi *et al*. (1998)	liq, melt	CRB72-151	0—3·0	53·80	1·13	15·19	9·40	0·16	6·12	10·09	2·88	0·69		0·26	99·72	53·7	1·75—2·25
		CRB75-219	0·25—2·25	51·52	1·70	14·98	11·83	0·18	5·96	9·71	2·76	0·60		0·32	99·56	47·3	2·0<
		CRB72-180	0—2·25	49·17	3·15	14·45	13·91	0·19	5·70	8·94	2·54	1·01		0·65	99·71	42·2	1·75—2·25
		CRB72-31	0—3·0	50·76	1·48	16·02	9·52	0·14	8·23	10·77	2·29	0·39		0·19	99·79	60·6	1·75—2·0
Tsuruta & Takahashi (1998)	sol, liq	JB1	0—12·5	53·25	1·37	14·83	8·36	0·17	7·89	9·48	2·85	1·46	0·05	0·26	99·97	62·7	
Wagner & Grove (1998)	liq, melt	Kilauea tholeiite	1·0—2·2	48·80	1·77	10·30	11·60	0·17	17·20	8·25	1·52	0·27			99·88	72·5	
Yaxley & Green (1998)	melt	GA1	3·5	50·35	1·49	16·53	9·83	0·17	7·94	9·60	3·49	0·44		0·16	100·01	59·0	
Kogiso & Hirschmann (2001)	sol, melt	Pyrox2B	1·0	51·56	0·54	5·58	7·01	0·10	16·19	18·18	0·84				100·00	80·5	
		OLCPX1	1·0—2·0	47·92	0·47	4·49	9·26	0·13	23·38	13·72	0·63				100·00	81·8	
		OLCPX2	1·0	48·73	0·39	4·13	7·93	0·12	24·42	13·71	0·57				100·00	84·6	
Kogiso & Hirschmann (2002)	sol, liq, melt	B-ECL1	5·0	46·43	1·73	15·46	10·89	0·20	9·95	12·79	2·52	0·00	0·03		100·00	62·0	
Pertermann & Hirschmann (2003*a*)	sol, liq, melt	G2	3·0	50·05	1·97	15·76	9·35	0·17	7·90	11·74	3·04	0·03			100·01	60·1	
Hirschmann *et al*. (2003) Kogiso *et al*. (2003)	sol, liq, melt	MIX1G	2·0—7·5	45·56	0·90	15·19	7·77	0·15	16·67	11·48	1·44	0·04	0·11	0·01	99·32	79·3	2·0—2·5
Peridotite—pyroxenite mixture																	
Kogiso *et al*. (1998)	melt	KG1	1·5—3·0	46·97	0·78	9·75	9·77		23·57	7·35	1·52	0·12	0·17		100·00	81·1	
		KG2	1·5—3·0	46·22	0·57	7·69	9·22		28·83	6·05	1·11	0·09	0·22		100·00	84·8	
Yaxley (2000)	sol, liq	GA1 + MPY90 3:1	3·5	48·95	1·15	13·49	9·27	0·16	15·61	8·05	2·72	0·33	0·11	0·11	99·95	75·0	
		GA1 + MPY90 1:1	3·5	47·55	0·83	10·45	8·70	0·14	23·26	6·49	1·95	0·22	0·23	0·07	99·89	82·7	
		GA1 + MPY90 3:5	3·5	46·84	0·66	8·93	8·41	0·13	27·09	5·71	1·56	0·17	0·28	0·05	99·83	85·2	
		GA1 + MPY90 1:3	3·5	46·14	0·50	7·41	8·12	0·13	30·92	4·94	1·17	0·11	0·34	0·20	99·98	87·2	

[1]Parameters determined in experiments: sol, solidus temperature; liq, liquidus temperature; melt, compositions of partial melts.
[2]Pressure range of experiments; '0' is 0·1 MPa.
[3]Lower pressure limit (GPa) of the appearance of the assemblage liquid + garnet + clinopyroxene ± orthopyroxene.
*Total iron given as FeO.

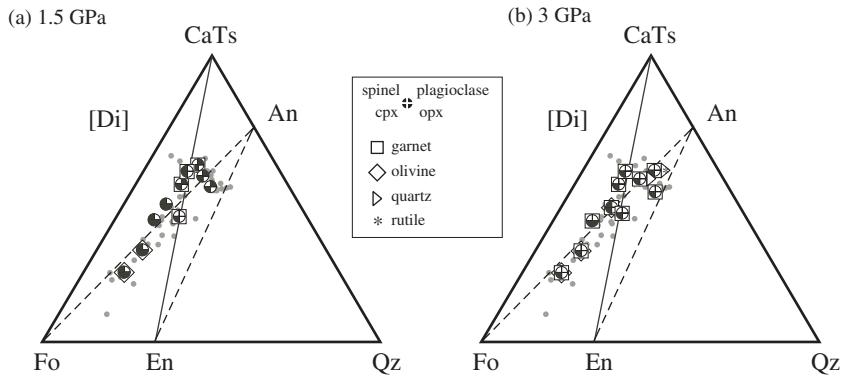

Fig. 3. Subsolidus phase assemblages of pyroxenites used for experimental studies (Table 1) in the pseudoternery Fo–CaTs–Qz diagram projected from [Di] at (a) 1·5 GPa and (b) 3·0 GPa. Phases present are indicated by filled split circles for spinel, plagioclase, orthopyroxene (opx) and clinopyroxene (cpx). Symbols for other phases are as in the inset. Small grey circles are compositions of pyroxenites for which subsolidus phases were not determined.

MELTING PHASE RELATIONS OF PYROXENITE

Following the pioneering experiments of Yoder & Tilley (1962), there have been numerous high-pressure studies on partial melting of mafic lithologies. Fundamental melting relations of mafic to ultramafic compositions for pressures ranging from 0·1 MPa to 3 GPa were documented in the 1960 s (e.g. Yoder & Tilley, 1962; Green & Ringwood, 1967; O'Hara, 1968). Later studies were conducted with a range of goals, such as determination of subsolidus phase relationships (e.g. Irving, 1974; Adam *et al.*, 1992), solidus and liquidus locations (e.g. Kornprobst, 1970; Yasuda *et al.*, 1994), or location of multiple saturation points of peridotite phases (e.g. Thompson, 1974, 1975; Eggins, 1992*a*; Kinzler & Grove, 1992). Newer experimental studies documented phase equilibria at pressures greater than 20 GPa (e.g. Yasuda *et al.*, 1994; Zhang & Herzberg, 1994; Hirose *et al.*, 1999). A number of recent studies have extended our knowledge of pyroxenite partial melt compositions (e.g. Kogiso & Hirschmann, 2001; Hirschmann *et al.*, 2003; Kogiso *et al.*, 2003; Pertermann & Hirschmann, 2003*a*). Nevertheless, individual studies generally focus on a restricted number of bulk compositions. In this paper, we survey these data to gain an overview of the role of source variation on the melting relations and partial melt compositions from pyroxenite source rocks. The experimental data considered in this paper are summarized in Table 1.

Phase assemblages from subsolidus to liquidus

Throughout this paper, we emphasize the primary influence of the garnet–pyroxene thermal divide, defined by the En–CaTs–Di plane in CMAS projections, on melting relations of pyroxenites. When projected into the Fo–CaTs–Qz–Di pseudoquaternary, the majority of pyroxenites project near this divide (Fig. 2), indicating that pyroxenes and garnet are commonly the predominant minerals under subsolidus conditions. Figure 3 shows subsolidus phase assemblages of various pyroxenites at different pressures. Clinopyroxene is stable in all, but orthopyroxene appears at relatively low pressures (<2 GPa) only in pyroxenites that project to compositions rich in En and poor in CaTs. Garnet appears as a subsolidus phase in pyroxenites of basaltic composition (poor in Fo component) at 1·5 GPa, and in nearly all compositions at 3·0 GPa. Accessory phases are quartz (or its high-pressure equivalent), feldspars and rutile in silica-excess pyroxenite, and olivine and spinels in silica-deficient pyroxenites (Fig. 3). Kyanite and sanidine are also observed in some silica-excess pyroxenites (grospydites, Smyth & Hatton, 1977), but such compositions have not been investigated experimentally. Silica-deficient pyroxenites have plagioclase only at pressures below the stability of garnet (Irving, 1974; Adam *et al.*, 1992). Corundum and ilmenite project on the thermal divide, and so in theory may occur in either silica-excess or silica-deficient pyroxenites. However, both phases imply low silica activity and are therefore more likely to be accessory minerals in silica-deficient varieties.

Based on experimental data of simple system (CMAS) and simple mixtures of natural minerals, O'Hara (1968) suggested that the garnet–pyroxene divide is stabilized at pressures above ~2·7 GPa, but later experiments on more complex compositions (Table 1) showed that the divide exists at lower pressures for natural rocks. The minimum pressures at which the assemblage liquid + garnet + clinopyroxene ± orthopyroxene appears are listed in Table 1. In many pyroxenite compositions, garnet and clinopyroxene (+ orthopyroxene) are the sole minerals in solid residues at pressures between ~1·5 and ~2·5 GPa. These pressures are lower than that

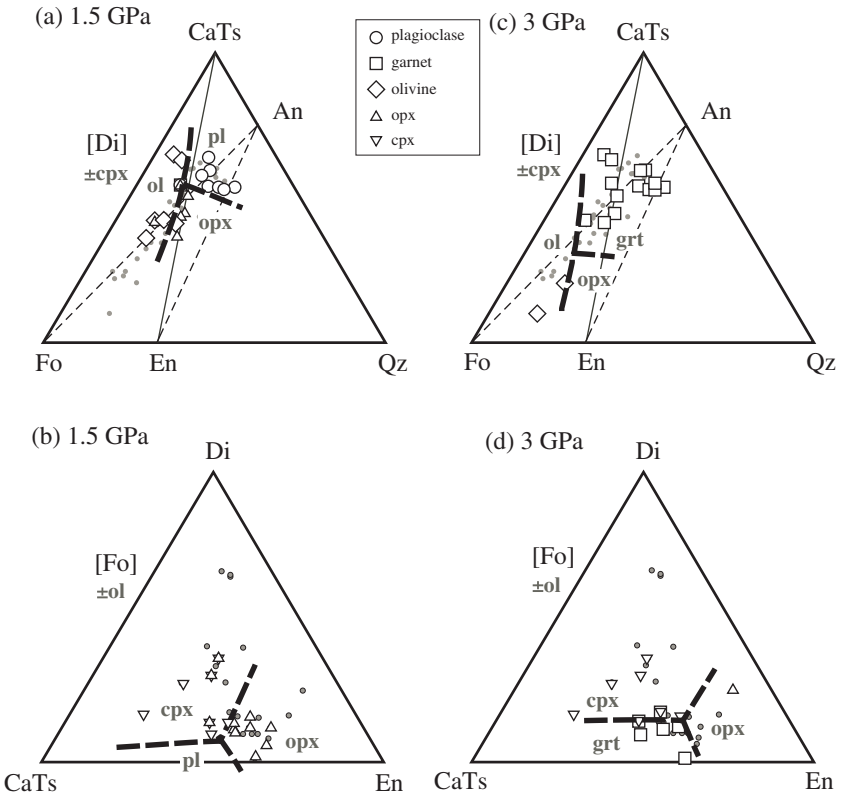

Fig. 4. Liquidus phases of pyroxenites determined in experiments at (a, b) 1·5 GPa and (c, d) 3·0 GPa. (a, c) Projection from [Di] onto the Fo–CaTs–Qz plane. (b, d) Projection from [Fo] onto the CaTs–Di–En plane, in which only silica-deficient compositions are shown. Bold dashed lines are estimated liquidus phase boundaries. Abbreviations are as in Fig. 2. Small grey circles are compositions of pyroxenites for which liquidus phases were not determined.

suggested by O'Hara (1968), primarily owing to the stabilizing effect of FeO on garnet (O'Neill, 1981). Thus, the silica-excess and silica-deficient classification of pyroxenites is applicable at pressure higher than ~2 GPa. Compositions of partial melts from silica-excess and silica-deficient compositions may be similar to one another at lower pressures, but may be controlled by thermal divides created on other mineral joins. For example, the Fo–An–Di plane (olivine–gabbro divide, O'Hara, 1968) is a divide that separates hypersthene- and quartz-normative liquids from nepheline-normative ones (Yoder & Tilley, 1962) at pressures between 0·1 MPa and 0·8 GPa (O'Hara, 1968).

The basic framework for understanding partial melting relations of pyroxenitic systems was established early in the history of high-pressure experimentation (e.g. Yoder & Tilley, 1962; Cohen *et al.*, 1967; Green & Ringwood, 1967; O'Hara, 1968). In particular, experiments in the CMAS system (e.g. O'Hara & Yoder, 1967; Kushiro, 1969; Presnall *et al.*, 1978; Milholland & Presnall, 1998; Liu & Presnall, 2000) have helped define mineral–melt phase relationships relevant to pyroxenitic (and peridotitic) systems for a wide range of pressure up to ~3 GPa. With increasing pressure, the chief features of this system in the Fo–CaTs–Qz–Di quaternary are: (1) the primary phase volume of olivine contracts; (2) the clinopyroxene phase volume expands towards the plagioclase and olivine phase volumes up to ~2·0 GPa; (3) the orthopyroxene phase volume expands toward the plagioclase and olivine phase volumes but shrinks back from the direction of the CaTs apex above ~2·0 GPa; (4) the primary phase volume of plagioclase is replaced by the phase volumes of spinel, sapphirine and corundum by ~2·0 GPa, above which the garnet phase volume appears and expands. Melting relations documented in experiments on natural materials largely follow these principles. Figure 4 shows liquidus phase boundaries projected into the Fo–CaTs–Qz–Di system estimated using experimental data from natural and near-natural compositions (Table 1). At 1·5 GPa, olivine is the liquidus phase for most silica-deficient pyroxenites, and clinopyroxene or plagioclase is the liquidus phase in silica-excess pyroxenites. At 3·0 GPa, garnet is the liquidus phase for a substantial range of pyroxenite compositions, including both silica-excess and silica-deficient varieties, and olivine appears on the liquidus only for near-peridotitic compositions. Orthopyroxene appears on the liquidus of pyroxenites that plot near the En apex mainly at $< \sim 2$ GPa.

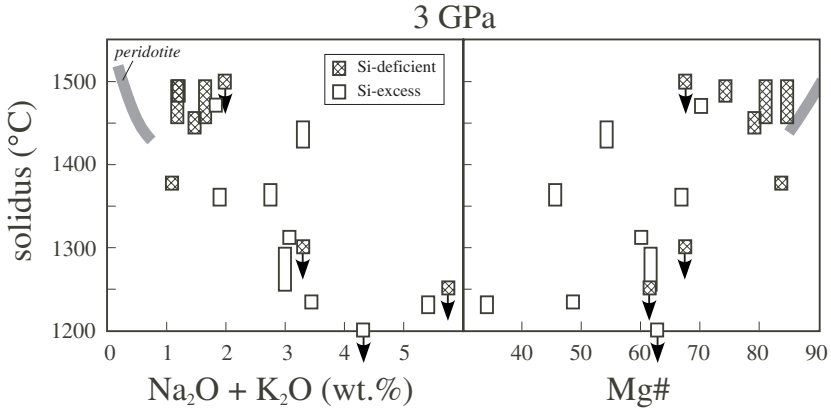

Fig. 5. Solidus temperatures of pyroxenite determined in experiments at 3·0 GPa as a function of bulk $Na_2O + K_2O$ and Mg-number content. Open and hatched rectangles are for silica-excess and silica-deficient pyroxenites, respectively. Rectangles with arrow indicate experiments in which the upper limit of the solidus temperature was determined. Wide grey lines are solidus temperature–bulk composition trends for peridotite (Hirschmann, 2000).

Quartz may appear on the liquidus in silica-excess pyroxenites that plot close to the Qz apex (Yaxley & Green, 1998), although such compositions are not within the range of natural pyroxenite.

Thus, when melting proceeds, residual phase assemblages change in accordance with bulk composition. For example, in silica-excess pyroxenite with MORB-like composition, the order of phase disappearance is quartz (or plagioclase)–garnet–clinopyroxene at 2–3 GPa (Pertermann & Hirschmann, 2003*a*) and coesite–clinopyroxene–garnet at 5 GPa (Yasuda *et al.*, 1994). In silica-deficient compositions at 2–3 GPa, olivine or spinel disappears first in pyroxenite with picritic (~16 wt % MgO) composition (Hirschmann *et al.*, 2003; Kogiso *et al.*, 2003), but olivine persists up to the liquidus in near-peridotitic compositions (Yaxley, 2000).

Solidus and liquidus temperatures

Pyroxenite solidus locations are also influenced significantly by bulk composition effects. In peridotitic compositions, alkali contents exert a strong influence on solidus temperatures, with Mg-number also playing a role (Walter & Presnall, 1994; Herzberg *et al.*, 2000; Hirschmann, 2000). These two variables also influence solidus temperatures of pyroxenite. Figure 5 shows variations in solidus temperatures at 3·0 GPa plotted against bulk composition. Although the data are rather scattered, solidus temperatures correlate negatively with bulk alkali content and positively with bulk Mg-number. It is impossible to separate the effect of these two variables on solidus temperatures because there is a strong negative correlation between bulk alkali content and Mg-number (Fig. 1). It should be noted that silica-excess and silica-deficient pyroxenites form similar trends, indicating that subsolidus phase assemblages do not have obvious influence on solidus temperatures.

Hirschmann (2000) argued that the alkali content of near-solidus liquids is the chief variable influencing peridotite solidus temperatures. This means that the effect of alkali content on solidus temperatures increases with bulk concentration but decreases with bulk partition coefficient; i.e. it is diminished with increased clinopyroxene mode or with increasing pressure, both of which render Na more compatible in the residue. An analogous relationship may apply to variations in solidus temperatures of pyroxenite, although data for near-solidus liquid compositions of pyroxenite are scarce. However, the effect of pressure may be distinct for pyroxenite. As in the case of peridotite, alkalis in pyroxenite become more compatible in clinopyroxene with increasing pressure, but clinopyroxene mode decreases in response to the expansion of garnet stability.

The slopes of the solidus temperature vs composition (alkali content or Mg-number) trends are similar for pyroxenite and peridotite lithologies (Fig. 5). Relative to those for peridotite, pyroxenite solidi are displaced to higher temperature at a given bulk alkali content or Mg-number. This difference may be related to the lower variance of peridotite, as originally suggested by O'Hara (1968). It may also partly be owing to differences in bulk partition coefficients for alkalis: at a given bulk alkali content, near-solidus liquid compositions will be more alkali-rich for peridotites. However, even though pyroxenites have a higher solidus temperature than peridotite at a given alkali content, most pyroxenites are much more alkali-rich than typical peridotites with 0·2–0·35 wt % $Na_2O + K_2O$. Thus, most pyroxenites have lower solidus temperatures than typical peridotite.

As is true for solidi, two broad compositional effects may influence liquidus temperatures of pyroxenite: the position in simple-system projections, and the combined effects of alkalis and Mg-number. The projected position

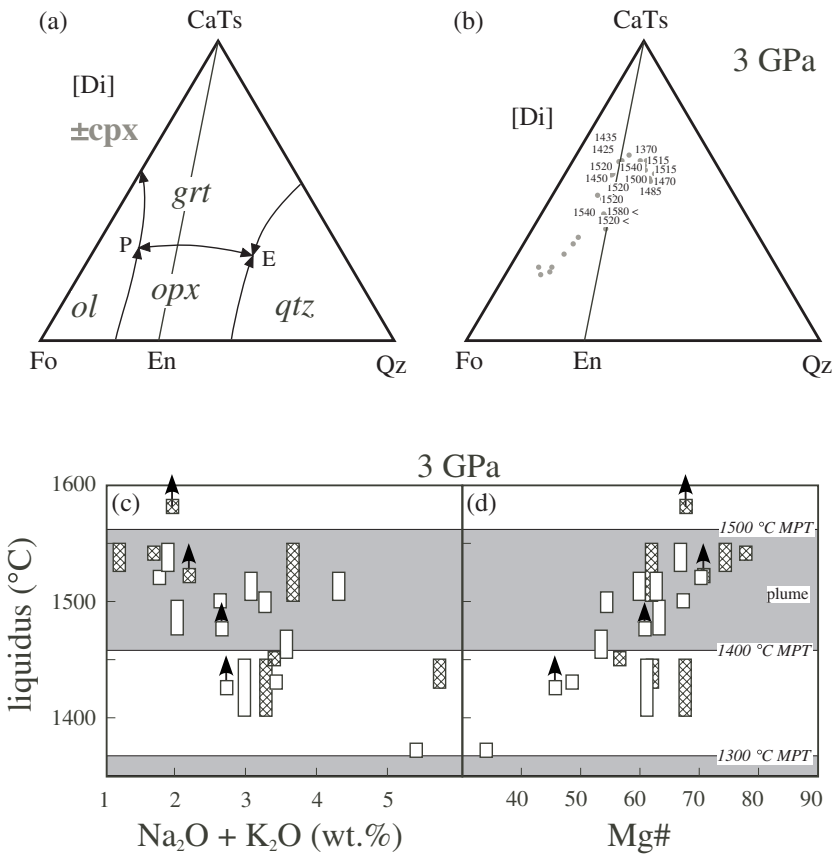

Fig. 6. (a) Schematic liquidus phase boundaries in the Fo–CaTs–Qz diagram projected from [Di]. Arrows show direction of falling temperature. Abbreviations are as in Fig. 2. (b–d) Liquidus temperatures of pyroxenites at 3 GPa projected from [Di] onto the Fo–CaTs–Qz plane (b), and plotted against bulk $Na_2O + K_2O$ and Mg-number content (c, d). Symbols are as in Fig. 5. Rectangles with arrow in (c) and (d) indicate experiments in which the lower limit of the liquidus temperature was determined. Also shown in (c) and (d) are temperature ranges of mantle with 1300°C and 1400–1500°C mantle potential temperature (MPT) at 3 GPa (Ita & Stixrude, 1992).

relative to the garnet–pyroxene thermal divide in the Fo–CaTs–Qz–Di system could influence the liquidus temperature because there is a thermal maximum along the CaTs–En join (Fig. 6a) in the true quaternary system Fo–CaTs–Qz projected from Di. Natural compositions projecting close to the thermal divide might be expected to have higher liquidus temperatures than those plotting far from it. However, as illustrated by Fig. 6b, such a relationship is not easily discerned from experiments on natural pyroxenites. Instead, there are clear correlations between liquidus temperature and bulk composition (Fig. 6c and d). The relative effects of the two variables are not distinguishable because of the strong correlation between bulk Mg-number and alkali content in pyroxenites (Fig. 1).

Comparison of the liquidus temperature of pyroxenites with geotherms applicable to basalt source regions indicates that many pyroxenites are completely molten at conditions expected where hot mantle plumes [$\sim$1500°C mantle potential temperature (MPT)] impinge on the oceanic lithosphere ($\sim$100 km). Thus, pyroxenites, if present in vigorous mantle plumes such as that inferred beneath Hawaii, should undergo nearly complete fusion. In contrast, many compositions will undergo only partial fusion for weaker plumes ($< \sim$1450°C MPT) or beneath mid-ocean ridges. It is these environments in which unusual compositions (such as highly alkalic partial melts of garnet pyroxenite or silicic partial melts of silica-saturated eclogite) may plausibly be of importance.

COMPOSITIONS OF PYROXENITE PARTIAL MELTS

Recent experimental studies on pyroxenite partial melting have reported compositions of partial melts produced from a range of bulk compositions under various pressure–temperature conditions (e.g. Kogiso *et al.*, 1998, 2003; Takahashi *et al.*, 1998; Tsuruta & Takahashi, 1998; Yaxley & Green, 1998; Hirschmann *et al.*, 2003; Pertermann & Hirschmann, 2003*a*). Compositions of experimental partial melts are variable, ranging from

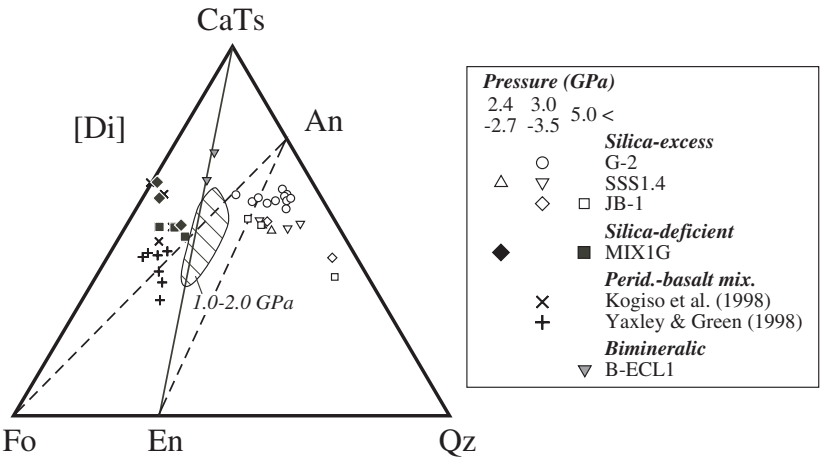

Fig. 7. Projection from [Di] onto the Fo–CaTs–Qz plane for compositions of pyroxenite partial melts produced in experiments at pressures at which garnet is stable. Hatched field is for partial melts from a silica-deficient pyroxenite (Kilauea tholeiite) produced under garnet-absent conditions at 1·0–2·0 GPa (Wagner & Grove, 1998).

basanitic to dacitic. In this section, we discuss systematic relationships between compositions of pyroxenite and their partial melts.

Role of the garnet–pyroxene thermal divide

The garnet–pyroxene thermal divide (Figs 2 and 6) has a critical influence on compositions of partial melts of pyroxenite. As described above, the significance of the thermal divide is that pyroxenites that reside on either side of the divide produce distinct types of partial melt when garnet and pyroxenes are the principal stable phases in the residue (O'Hara, 1968). This relationship is shown schematically in Fig. 6a for the quaternary Fo–CaTs–Qz–Di system. Silica-rich initial melts from silica-excess pyroxenites plot at the invariant point E on the silica-rich side of the thermal divide (Fig. 6). For silica-deficient pyroxenites, initial silica-poor melts form near an invariant point P, which may be a peritectic in which orthopyroxene reacts with liquid around 3 GPa (Longhi, 1995; Walter, 1998). Therefore, partial melts produced at low degrees of melting may migrate along the garnet–olivine–clinopyroxene cotectic until they reach point P (Fig. 6). Importantly, with progressive degrees of melting for both silica-excess and silica-deficient compositions, partial melts will not cross the boundary defined by the divide.

The garnet–pyroxene thermal divide is relevant to partial melting in natural pyroxenites. Figure 7 shows compositions of partial melts produced experimentally from different bulk compositions under conditions where clinopyroxene and garnet are the principal subsolidus phases. As in the case of simple systems, partial melts from silica-excess pyroxenites are silica-rich and those from silica-deficient pyroxenites are silica-poor at $> \sim 2$ GPa. Bimineralic pyroxenite (B-ECL1: Kogiso & Hirschmann, 2002) resides on the boundary between silica-excess and silica-deficient compositions, and its partial melts are also on the boundary (Fig. 7), consistent with this join acting as a thermal crest. It should be noted that the key influence of this thermal crest for each individual bulk composition is not in conflict with the observation that the thermal divide does not correspond to a maximum in liquidus temperatures of a range of pyroxenite bulk compositions (Fig. 6). Variations in Mg-number and alkali content affect the liquidus temperatures of different compositions (Fig. 6), but these compositional variables are not represented by the CMAS projection. For a bulk composition with any given Mg-number and alkali content, the chemography of melting is chiefly determined by its position relative to the thermal divide.

Major element compositions of partial melts

Figure 8 illustrates oxide contents of pyroxenite partial melts experimentally produced at pressures under which garnet is stable. Partial melts from silica-excess pyroxenites have >50 wt % SiO_2, and those from silica-deficient pyroxenites have <48 wt % (Fig. 8a). Partial melts of silica-excess pyroxenites are characterized by low MgO contents and Mg-numbers and are therefore very unlike partial melts of peridotite. In contrast, partial melts of silica-deficient pyroxenites can be rather primitive, with MgO of 12–16 wt % and Mg-number between 60 and 75, and thus have broad similarities to partial melts of peridotite. In fact, partial melts of the two lithologies can overlap for many oxides, but those of silica-deficient pyroxenite tend to have higher FeO, TiO_2 and Na_2O, and lower SiO_2 (at a given MgO concentration). CaO and Al_2O_3 are more variable, being either higher or lower than for partial melts of peridotite.

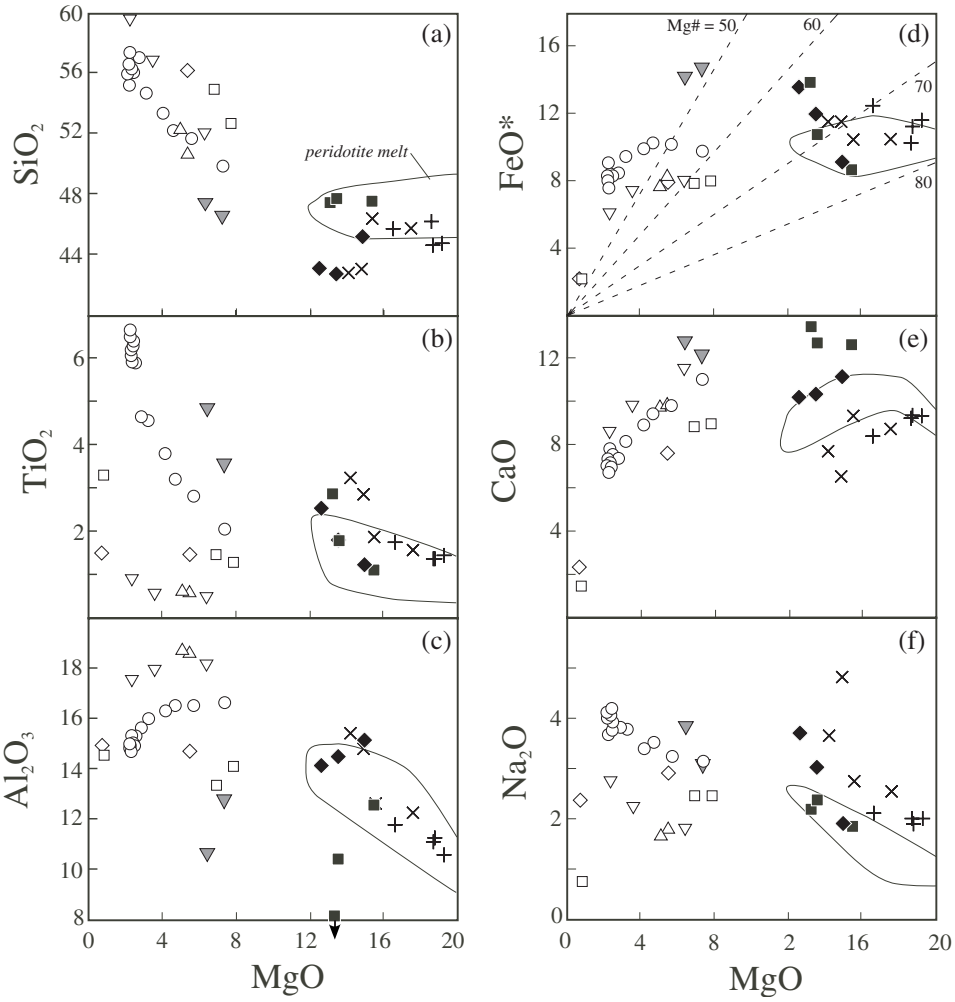

Fig. 8. Oxide compositions of experimentally produced partial melts of pyroxenite at pressures at which garnet is stable. Also shown is the field of peridotite partial melts produced at >2·5 GPa (Hirose & Kushiro, 1993; Kushiro, 1996; Walter, 1998). Symbols are as in Fig. 7. Mg-numbers are indicated with dashed lines in the MgO–FeO plot.

An important difference between the melting relations of silica-deficient pyroxenite and those of peridotite is evident in their respective MgO–Al_2O_3 systematics (Fig. 9). With increasing pressure or degree of melting, partial melts of peridotite become less aluminous and richer in MgO. Partial melts of silica-deficient pyroxenite also become less aluminous with increasing pressure, but may have negligible changes in MgO. These differences are owing to the distinct roles of olivine and garnet in the respective lithologies (Kogiso *et al.*, 2003). With increasing pressure, garnet becomes increasingly stable whereas olivine becomes less so. For a pyroxenite with little or no residual olivine, such as in MIX1G (Hirschmann *et al.*, 2003; Kogiso *et al.*, 2003), partial melts have less Al_2O_3 at higher pressures but show little variation in MgO (Fig. 9). In contrast, olivine contributes more to partial melts of garnet peridotite with increasing pressure (or increasing degree of melting), resulting in Al_2O_3-poor, MgO-rich liquids (Fig. 9). Partial melts of olivine-rich pyroxenite such as KG1 (peridotite + MORB 1:1 mixture, Kogiso *et al.*, 1998) follow the same MgO–Al_2O_3 trend as garnet peridotite melt (Fig. 8c), as they are also controlled by garnet and olivine.

Another consequence of enhanced garnet stability to the phase relations is relative contraction of clinopyroxene stability, which results in higher CaO/Al_2O_3 ratios of partial melts of garnet pyroxenite and garnet peridotite with increasing pressure (Fig. 9). However, just as for MgO–Al_2O_3 trends, increased CaO/Al_2O_3 can be accompanied by negligible MgO increases for olivine-poor lithologies, but not for peridotite.

PYROXENITE IN BASALT GENESIS

Here we discuss some potential ramifications of pyroxenite partial melting to the genesis of OIB magmas.

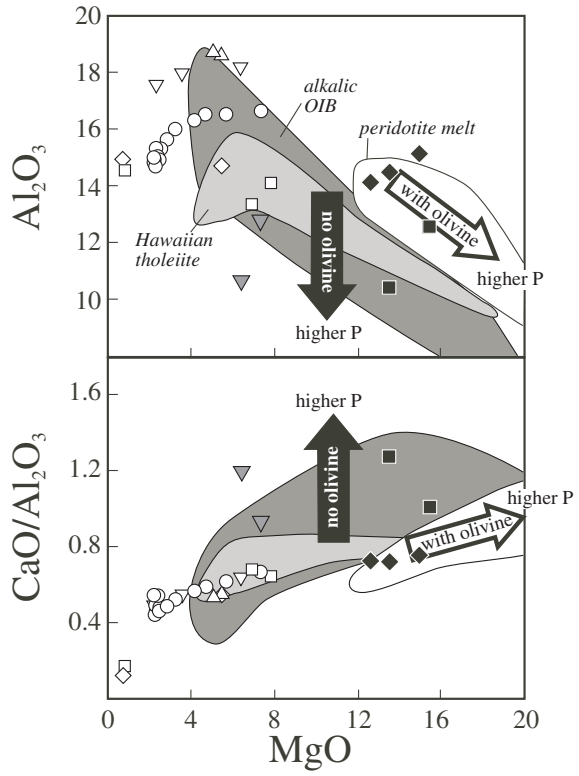

Fig. 9. Comparison of Al_2O_3 contents and CaO/Al_2O_3 ratios for pyroxenite partial melts, peridotite partial melts, and OIB. Dark and light shaded fields are of nepheline-normative OIB lavas from several hotspots (Canary, Azores, St. Helena, Tristan da Cunha, Marquesas, Society, Cook–Austral, Pitcairn–Gambier, and Samoa) and hypersthene-normative lavas from Hawaiian shield volcanoes, respectively. Data are from the GEOROC database (available at http://georoc.mpch-mainz.dwdg.de). Arrows indicate composition shifts with increasing pressure for partial melts produced in the presence (white) and absence (black) of olivine. Symbols are experimental partial melts from pyroxenites as in Fig. 7.

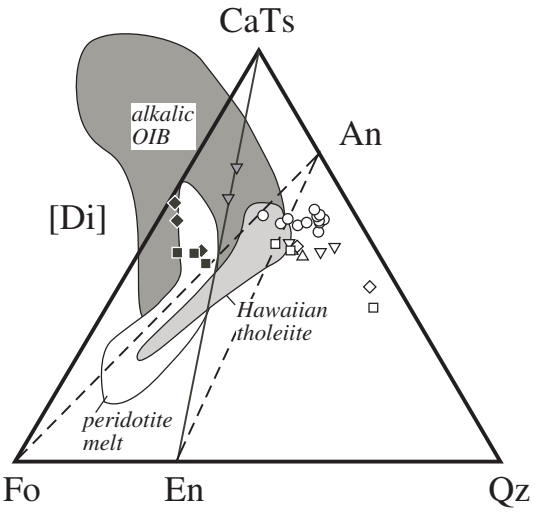

Fig. 10. Comparison of pyroxenite partial melts, peridotite partial melts, and OIB in the Fo–CaTs–Qz diagram projected from [Di]. Symbols are as in Fig. 7

Detailed consideration of the link between pyroxenite partial melts and MORB genesis has been addressed elsewhere (Hirschmann & Stolper, 1996; Pertermann & Hirschmann, 2003*a*, 2003*b*).

OIB lavas from many hotspots have nepheline-normative (alkali basaltic) compositions (Hirschmann *et al.*, 2003; Kogiso *et al.*, 2003), whereas those from some hotspots, such as Hawaii, are dominated by hypersthene-normative (tholeiitic) compositions (Fig. 10). The conventional view for the origin of these two types of OIB is that they are generated by partial melting of peridotite at different degrees of melting (e.g. Chen & Frey, 1985; Wyllie, 1988; McKenzie & O'Nions, 1991). However, both alkali basaltic and tholeiitic OIB lavas are characterized by lower Al_2O_3 contents compared with experimentally derived partial melts of peridotite (Fig. 9), suggesting that OIB lavas are not produced simply from peridotite partial melting (Hirschmann *et al.*, 2003; Kogiso *et al.*, 2003). Parameterization of experimental data of peridotite partial melting (Herzberg & O'Hara, 2002) demonstrates that near-solidus partial melts of peridotite produced around 4 GPa have low Al_2O_3 contents comparable with plausible parental liquids for OIB. The correspondence between such liquids and alkalic OIB merits further investigation. However, tholeiitic OIB are generally thought to derive from high-degree partial melts of peridotite, which do not have low Al_2O_3. For example, the parameterization of Herzberg & O'Hara (2002, appendix 6) posits that parental liquids for tholeiitic OIB equilibrate with harzburgite residue, which requires relatively high degrees of partial melting. Also, near-solidus melts from peridotite may have relatively low SiO_2 contents (Herzberg & O'Hara, 2002), but they are not as low in SiO_2 as alkalic OIB lavas are (Kogiso *et al.*, 2003). Partial melting of peridotite + CO_2 can produce liquids with extremely low SiO_2 contents (Hirose, 1997), but it cannot explain relatively high FeO contents of OIB (Kogiso *et al.*, 1998, 2003). Problems in generation of alkalic OIB lavas with regard to peridotite melting have been addressed in detail by Kogiso *et al.* (2003).

Alternatively, OIB lavas may be generated by partial melting of pyroxenite, or may incorporate a pyroxenite-derived component. As mentioned above, nepheline-normative compositions are dominant in many OIB suites. Many partial melts of silica-deficient pyroxenite plot on the left side of the Fo–An join, and consequently are nepheline-normative (Figs 7 and 10). Also, as described above, if olivine is absent in partially melting pyroxenite, high-pressure partial melts from silica-deficient pyroxenite have systematically lower Al_2O_3 contents than peridotite melts at a given MgO content (Fig. 9). In fact, melts produced from a silica-deficient pyroxenite MIX1G at

5 GPa (Kogiso *et al.*, 2003) are sufficiently low in Al_2O_3 to be plausible parents to primitive OIB lavas (Fig. 9). Thus, it is possible that magmas similar to parental liquids for alkalic OIB are produced by partial melting of silica-deficient pyroxenite if the residue contains significant garnet and lacks olivine.

Tholeiitic OIB magmas might incorporate a component of partial melts from silica-excess pyroxenite. Such partial melts are generally hypersthene-normative to quartz-normative (Figs 7 and 10), and their Al_2O_3 contents are as low as OIB (Fig. 9). Silica-excess pyroxenite melts are too low in MgO and Fo components to be parental to hypersthene-normative OIB, and therefore Niu & O'Hara (2003) argued that partial melting of recycled MORB crust is not suitable to be a source for tholeiitic OIB. However, mixing of silica-excess pyroxenite melts with MgO-rich melts produced from peridotite may plausibly account for the compositions of tholeiitic OIB (Figs 9 and 10).

It is still possible that the low-Al_2O_3 signature of tholeiitic OIB results from partial melting of Al-depleted peridotite compositions, such as harzburgite, because the Al_2O_3 content of partial melt may depend on that of source peridotite (Herzberg & O'Hara, 2002). Some experimental data also demonstrate that parental liquids for tholeiitic OIB can be in equilibrium with harzburgite residue (Eggins, 1992*a*; Wagner & Grove, 1998). However, natural harzburgite generally has a refractory character and is strongly depleted in incompatible elements, so it is not a plausible lithology as a source for OIB lavas that are enriched in incompatible elements much more than MORB. This discrepancy might be explained by rather complex scenarios, such as dynamic melting processes (Eggins, 1992*b*) in which the bulk composition of the parental melt is determined by phase equilibrium with harzburgite at the shallowest level of melting, with enrichment in incompatible elements produced by smaller-degree melt fractions from deeper level. Similar results might be obtained by low-pressure melt–rock reaction of a melt generated at high pressure (Wagner & Grove, 1998).

ACKNOWLEDGEMENTS

We are grateful to Yaoling Niu for inviting us to contribute to this volume in honor of Mike O'Hara. In this paper and countless other experimental studies, the ample use of projections pioneered by O'Hara is but one expression of his remarkable legacy. We also acknowledge constructive reviews by Claude Herzberg, Michael Walter, and an anonymous reviewer. Significant support for this project came from a MEXT grant 15740318 to T.K. and NSF grants OCE 9706526 and OCE9876255 to M.M.H.

REFERENCES

Adam, J., Green, T. H. & Day, R. A. (1992). An experimental study of two garnet pyroxenite xenoliths from the Bullenmerri and Gnotuk Maars of western Victoria, Australia. *Contributions to Mineralogy and Petrology* **111**, 505–514.

Arculus, R. J. (1975). Melting behavior of two basanites in the range 10–35 kbar and the effect of TiO_2 on the olivine–diopside reactions at high pressures. *Carnegie Institution of Washington Yearbook* **74**, 512–515.

Arndt, N. T. & Goldstein, S. L. (1989). An open boundary between lower continental crust and mantle: its role in crust formation and crustal recycling. *Tectonophysics* **161**, 201–212.

Baker, M. B. & Stolper, E. M. (1994). Determining the composition of high-pressure mantle melts using diamond aggregates. *Geochimica et Cosmochimica Acta* **58**, 2811–2827.

Chase, C. G. (1981). Oceanic island Pb: two-stage histories and mantle evolution. *Earth and Planetary Science Letters* **52**, 227–284.

Chen, C.-Y. & Frey, F. A. (1985). Trace element and isotopic geochemistry of lavas from Haleakala Volcano, East Maui, Hawaii: implications for the origin of Hawaiian basalts. *Journal of Geophysical Research* **90**, 8743–8768.

Class, C. & Goldstein, S. L. (1997). Plume–lithosphere interactions in the ocean basins: constraints from the source mineralogy. *Earth and Planetary Science Letters* **150**, 245–260.

Cohen, L. H., Ito, K. & Kennedy, G. C. (1967). Melting and phase relations in an anhydrous basalt to 40 kilobars. *American Journal of Science* **265**, 475–518.

Dick, H. J. B., Bloomer, S. H., Kirby, S. H., Stakes, D. S. & Mawer, C. K. (1991). Lithostratigraphic evolution of an in-situ section of oceanic layer 3. In: Von Herzen, R. P., Robinson, P. T., Adamson, A. C., *et al.* (eds) *Proceedings of the Ocean Drilling Program, Scientific Results, 118*. College Station, TX: Ocean Drilling Program, pp. 439–538.

Eggins, S. M. (1992*a*). Petrogenesis of Hawaiian tholeiites: 1, phase equilibria constraints. *Contributions to Mineralogy and Petrology* **110**, 387–397.

Eggins, S. M. (1992*b*). Petrogenesis of Hawaiian tholeiites: 2, aspects of dynamic melt segregation. *Contributions to Mineralogy and Petrology* **110**, 398–410.

Falloon, T. J. & Green, D. H. (1988). Anhydrous partial melting of peridotite from 8 to 35 kb and the petrogenesis of MORB. *Journal of Petrology, Special Lithosphere Issue*, 379–414.

Green, D. H. & Ringwood, A. E. (1967). The genesis of basaltic magmas. *Contributions to Mineralogy and Petrology* **15**, 103–190.

Halliday, A. N., Lee, D.-C., Tommasini, S., Davies, G. R., Paslick, C. R., Fitton, J. G. & James, D. E. (1995). Incompatible trace elements in OIB and MORB and source enrichment in the sub-oceanic mantle. *Earth and Planetary Science Letters* **133**, 379–395.

Hauri, E. H. (1996). Major-element variability in the Hawaiian mantle plume. *Nature* **382**, 415–419.

Hekinian, R., Bideau, D., Francheteau, J., Cheminee, J. L., Armijo, R., Lonsdale, P. & Blum, N. (1993). Petrology of the East Pacific Rise crust and upper mantle exposed in Hess Deep (eastern Equatorial Pacific). *Journal of Geophysical Research* **98**, 8069–8094.

Helffrich, G. R. & Wood, B. J. (2001). The Earth's mantle. *Nature* **412**, 501–507.

Herzberg, C. & O'Hara, M. J. (2002). Plume-associated ultramafic magmas of Phanerozoic age. *Journal of Petrology* **43**, 1857–1883.

Herzberg, C., Feigenson, M., Skuba, C. & Ohtani, E. (1988). Majorite fractionation recorded in the geochemistry of peridotites from South Africa. *Nature* **332**, 823–826.

Herzberg, C., Raterron, P. & Zhang, J. (2000). New experimental observations on the anhydrous solidus for peridotite KLB-1. *Geochemistry, Geophysics, Geosystems* **1**, 2000GC000089.

Hirose, K. (1997). Partial melt compositions of carbonated peridotite at 3 GPa and role of CO_2 in alkali-basalt magma generation. *Geophysical Research Letters* **24**, 2837–2840.

Hirose, K. & Kushiro, I. (1993). Partial melting of dry peridotites at high pressures: determination of compositions of melts segregated from peridotite using aggregates of diamond. *Earth and Planetary Science Letters* **114**, 477–489.

Hirose, K., Fei, Y., Ma, Y. & Mao, H.-K. (1999). The fate of subducted basaltic crust in the Earth's lower mantle. *Nature* **396**, 53–56.

Hirschmann, M. M. (2000). The mantle solidus: experimental constraints and the effect of peridotite composition. *Geochemistry, Geophysics, Geosystems* **1**, 2000GC000070.

Hirschmann, M. M. & Stolper, E. M. (1996). A possible role for garnet pyroxenite in the origin of the 'garnet signature' in MORB. *Contributions to Mineralogy and Petrology* **124**, 185–208.

Hirschmann, M. M., Kogiso, T., Baker, M. B. & Stolper, E. M. (2003). Alkalic magmas generated by partial melting of garnet pyroxenite. *Geology* **31**, 481–484.

Hofmann, A. W. (1997). Mantle geochemistry: the message from oceanic volcanism. *Nature* **385**, 219–229.

Hofmann, A. W. & White, W. M. (1982). Mantle plumes from ancient oceanic crust. *Earth and Planetary Science Letters* **57**, 421–436.

Irving, A. J. (1974). Geochemical and high pressure experimental studies of garnet pyroxenite and pyroxene granulite xenoliths from the Delegate basaltic pipes, Australia. *Journal of Petrology* **15**, 1–40.

Ita, J. & Stixrude, L. (1992). Petrology, elasticity, and composition of the mantle transition zone. *Journal of Geophysical Research* **97**, 6849–6866.

Ito, K. & Kennedy, G. C. (1974). The composition of liquids formed by partial melting of eclogites at high temperatures and pressures. *Journal of Geology* **82**, 383–392.

Iwamori, H., McKenzie, D. & Takahashi, E. (1995). Melt generation by isentropic mantle upwelling. *Earth and Planetary Science Letters* **134**, 253–266.

Jaques, A. L. & Green, D. H. (1980). Anhydrous melting of peridotite at 0–15 kb pressure and the genesis of tholeiitic basalts. *Contributions to Mineralogy and Petrology* **73**, 287–310.

Johnston, A. D. (1986). Anhydrous *P–T* phase relations of near-primary high-alumina basalt from the South Sandwich Islands: implications for the origin of island arcs and tonalite–trondhjemite series rocks. *Contributions to Mineralogy and Petrology* **92**, 368–382.

Jull, M. & Kelemen, P. B. (2001). On the conditions for lower crustal convective instability. *Journal of Geophysical Research* **106**, 6423–6446.

Kelemen, P. B., Hirth, G., Shimizu, N., Spiegelman, M. & Dick, H. J. B. (1997). A review of melt migration processes in the adiabatically upwelling mantle beneath oceanic spreading ridges. *Philosophical Transactions of the Royal Society of London, Series A* **355**, 283–318.

Kinzler, R. J. (1997). Melting of mantle peridotite at pressures approaching the spinel to garnet transition: application to mid-ocean ridge basalt petrogenesis. *Journal of Geophysical Research* **102**, 853–874.

Kinzler, R. J. & Grove, T. L. (1992). Primary magmas of mid-ocean ridge basalts 1. Experiments and methods. *Journal of Geophysical Research* **97**, 6885–6906.

Klein, E. M. & Langmuir, C. H. (1987). Global correlations of ocean ridge basalt chemistry with axial depth and crustal thickness. *Journal of Geophysical Research* **92**, 8089–8115.

Kogiso, T. & Hirschmann, M. M. (2001). Experimental study of clinopyroxenite partial melting and the origin of ultra-calcic melt inclusions. *Contributions to Mineralogy and Petrology* **142**, 347–360.

Kogiso, T. & Hirschmann, M. M. (2002). Partial melting experiments of bimineralic eclogite and the origin of ocean island basalts. *EOS Transactions, American Geophysical Union* **83**, Abstract V71C-12.

Kogiso, T., Tatsumi, Y., Shimoda, G. & Barsczus, H. G. (1997). High μ (HIMU) ocean island basalts in southern Polynesia: new evidence for whole-mantle scale recycling of subducted oceanic crust. *Journal of Geophysical Research* **102**, 8085–8103.

Kogiso, T., Hirose, K. & Takahashi, E. (1998). Melting experiments on homogeneous mixtures of peridotite and basalt: application to the genesis of ocean island basalts. *Earth and Planetary Science Letters* **162**, 45–61.

Kogiso, T., Hirschmann, M. M. & Frost, D. J. (2003). High pressure partial melting of garnet pyroxenite: possible mafic lithologies in the source of ocean island basalts. *Earth and Planetary Science Letters* **216**, 603–617.

Komiya, T., Hayashi, M., Maruyama, S. & Yurimoto, H. (2002*a*). Intermediate-*P/T* type Archean metamorphism of the Isua supracrustal belt: implications for secular change of geothermal gradients at subduction zones and for Archean plate tectonics. *American Journal of Science* **302**, 806–826.

Komiya, T., Maruyama, S., Hirata, T. & Yurimoto, H. (2002*b*). Petrology and geochemistry of MORB and OIB in the mid-Archean North Pole region, Pilbara craton, Western Australia: implications for the composition and temperature of the upper mantle at 3·5 Ga. *International Geology Review* **44**, 988–1016.

Kornprobst, J. (1970). Les péridotites et les pyroxénolites du massif ultrabasique des Beni Bouchera: une étude expérimentale entre 1100 et 1550°C, sous 15 à 30 kilobars de pression sèche. *Contributions to Mineralogy and Petrology* **29**, 290–309.

Kornprobst, J. (1977). A subsolidus high-pressure/high temperature experimental study on a garnet websterite assemblage exsolved from a single clinopyroxene accumulate at Freychinede (an alpine-type peridotite body, Northern French Pyrenees). *Colloques Internationaux du CNRS* **272**, 245–251.

Kushiro, I. (1969). The system forsterite–diopside–silica with and without water at high pressures. *American Journal of Science* **267A**, 269–294.

Kushiro, I. (1996). Partial melting of a fertile mantle peridotite at high pressures: an experimental study using aggregates of diamond. In: Basu, A. & Hart, S. (eds) *Earth Processes: Reading the Isotopic Code*. Washington, DC: American Geophysical Union, pp. 109–122.

le Roux, P. J., le Roex, A. P. & Schilling, J. G. (2002). MORB melting processes beneath the southern Mid-Atlantic Ridge (40–55°S): a role for mantle plume-derived pyroxenite. *Contributions to Mineralogy and Petrology* **144**, 206–229.

Liu, T.-C. & Presnall, D. C. (2000). Liquidus phase relations in the system CaO–MgO–Al_2O_3–SiO_2 at 2·0 GPa: applications to basalt formation, eclogites, and igneous sapphirine. *Journal of Petrology* **41**, 3–20.

Longhi, J. (1995). Liquidus equilibria of some primary lunar and terrestrial melts in the garnet stability field. *Geochimica et Cosmochimica Acta* **59**, 2375–2386.

McDonough, W. F. & Sun, S.-s. (1995). The composition of the Earth. *Chemical Geology* **120**, 223–253.

McKenzie, D. & Bickle, M. J. (1988). The volume and composition of melt generated by extension of the lithosphere. *Journal of Petrology* **29**, 625–679.

McKenzie, D. & O'Nions, R. K. (1991). Partial melt distributions from inversion of rare earth element concentrations. *Journal of Petrology* **32**, 1021–1091.

Melson, W. G., O'Hearn, T. & Kimberly, P. (1999). Volcanic glasses from sea-floor spreading centers and other deep sea tectonic settings: major and minor element compositions in the Smithsonian WWW

Data Set (abstract). *EOS Transactions, American Geophysical Union* **80**, F1177.

Michael, P. J., Langmuir, C. H., Dick, H. J. B., Show, J. E., Goldstein, S. L., Graham, D. W., Lehnert, K., Kurras, G., Jokat, W., Mühe, R. & Edmonds, H. N. (2003). Magmatic and amagmatic seafloor generation at the ultraslow-spreading Gakkel ridge, Arctic Ocean. *Nature* **423**, 956–961.

Milholland, C. S. & Presnall, D. C. (1998). Liquidus phase relations in the CaO–MgO–Al_2O_3–SiO_2 system at 3·0 GPa; the aluminous pyroxene thermal divide and high-pressure fractionation of picritic and komatiitic magmas. *Journal of Petrology* **39**, 3–27.

Niu, Y. & O'Hara, M. J. (2003). Origin of ocean island basalts: a new perspective from petrology, geochemistry, and mineral physics considerations. *Journal of Geophysical Research* **108**, 10.1029/2002JB002048.

O'Hara, M. J. (1968). The bearing of phase equilibria studies in synthetic and natural systems on the origin and evolution of basic and ultrabasic rocks. *Earth-Science Reviews* **4**, 69–133.

O'Hara, M. J. & Yoder, H. S., Jr (1967). Formation and fractionation of basic magmas at high pressures. *Scottish Journal of Geology* **3**, 67–117.

O'Neill, H. S. C. (1981). The transition between spinel lherzolite and garnet lherzolite and its use as a geobarometer. *Contributions to Mineralogy and Petrology* **77**, 185–194.

Obata, M. & Dickey, J. S., Jr (1976). Phase relations of mafic layers in the Ronda peridotite. *Carnegie Institution of Washington Yearbook* **75**, 562–566.

Pertermann, M. & Hirschmann, M. M. (2003*a*). Anhydrous partial melting experiments on MORB-like eclogite: phase relations, phase compositions and mineral–melt partitioning of major elements at 2–3 GPa. *Journal of Petrology* **44**, 2173–2201.

Pertermann, M. & Hirschmann, M. M. (2003*b*). Partial melting experiments on a MORB-like pyroxenite between 2 and 3 GPa: constraints on the presence of pyroxenites in basalt source regions from solidus location and melting rate. *Journal of Geophysical Research* **108**, 2125, doi: 10.1029/2000JB000118.

Presnall, D. C., Dixon, S. A., Dixon, J. R., O'Donnell, T. H., Brenner, N. L., Schrock, R. L. & Dycus, D. W. (1978). Liquidus phase relations on the join diopside–forsterite–anorthite from 1 atm to 20 kbar; their bearing on the generation and crystallization of basaltic magma. *Contributions to Mineralogy and Petrology* **66**, 203–220.

Ringwood, A. E. (1975). *Composition and Petrology of the Earth's Mantle*. New York: McGraw–Hill.

Rudnick, R. L., Barth, M., Horn, I. & McDonough, W. F. (2000). Rutile-bearing refractory eclogites: missing link between continents and depleted mantle. *Science* **287**, 278–281.

Salters, V. J. M. & Dick, H. J. B. (2002). Mineralogy of the mid-ocean-ridge basalt source from neodymium isotopic composition of abyssal peridotites. *Nature* **418**, 68–72.

Schulze, D. J. (1989). Constraints on the abundance of eclogite in the upper mantle. *Journal of Geophysical Research* **94**, 4205–4212.

Smyth, J. R. & Hatton, C. J. (1977). A coesite–sanidine grospydite from the Roberts Victor kimberlite. *Earth and Planetary Science Letters* **34**, 284–290.

Stracke, A., Salters, V. J. M. & Sims, K. W. W. (1999). Assessing the presence of garnet-pyroxenite in the mantle sources of basalts through combined hafnium–neodymium–thorium isotope systematics. *Geochemistry, Geophysics, Geosystems* **1**, 1999GC000013.

Takahashi, E. & Kushiro, I. (1983). Melting of a dry peridotite at high pressures and basalt magma genesis. *American Mineralogist* **68**, 859–879.

Takahashi, E. & Nakajima, K. (2002). Melting process in the Hawaiian plume: an experimental study. In: Takahashi, E., Lipman, P. W., Garcia, M., Naka, J. & Aramaki, S. (eds) *Hawaiian Volcanoes: Deep Underwater Perspectives*. Washington, DC: American Geophysical Union, pp. 403–418.

Takahashi, E., Nakajima, K. & Wright, T. L. (1998). Origin of the Columbia River basalts: melting model of a heterogeneous plume head. *Earth and Planetary Science Letters* **162**, 63–80.

Thompson, R. N. (1974). Primary basalts and magma genesis I. Skye, North-west Scotland. *Contributions to Mineralogy and Petrology* **45**, 317–341.

Thompson, R. N. (1975). Primary basalts and magma genesis II. Snake River Plain, Idaho, U.S.A. *Contributions to Mineralogy and Petrology* **52**, 213–232.

Tsuruta, K. & Takahashi, E. (1998). Melting study of an alkali basalt JB-1 up to 12·5 GPa: behavior of potassium in the deep mantle. *Physics of the Earth and Planetary Interiors* **107**, 119–130.

Wagner, T. P. & Grove, T. L. (1998). Melt/harzburgite reaction in the petrogenesis of tholeiitic magma from Kilauea volcano, Hawaii. *Contributions to Mineralogy and Petrology* **131**, 1–12.

Walter, M. J. (1998). Melting of garnet peridotite and the origin of komatiite and depleted lithosphere. *Journal of Petrology* **39**, 29–60.

Walter, M. J. & Presnall, D. C. (1994). Melting behavior of simplified lherzolite in the system CaO–MgO–Al_2O_3–SiO_2–Na_2O from 7 to 35 kbar. *Journal of Petrology* **35**, 329–359.

Wei, K., Trønnes, R. G. & Scarfe, C. M. (1990). Phase relations of aluminum-undepleted and aluminum-depleted komatiites at pressures of 4–12 GPa. *Journal of Geophysical Research* **95**, 15817–15827.

Wyllie, P. J. (1988). Solidus curves, mantle plumes, and magma generation beneath Hawaii. *Journal of Geophysical Research* **93**, 4171–4181.

Yasuda, A., Fujii, T. & Kurita, K. (1994). Melting phase relations of an anhydrous mid-ocean ridge basalt from 3 to 20 GPa: implications for the behavior of subducted oceanic crust in the mantle. *Journal of Geophysical Research* **99**, 9401–9414.

Yaxley, G. M. (2000). Experimental study of the phase and melting relations of homogeneous basalt + peridotite mixtures and implications for the petrogenesis of flood basalts. *Contributions to Mineralogy and Petrology* **139**, 326–338.

Yaxley, G. M. & Green, D. H. (1998). Reactions between eclogite and peridotite: mantle refertilisation by subduction of oceanic crust. *Schweizerische Mineralogische und Petrographische Mitteilungen* **78**, 243–255.

Yoder, H. S., Jr & Tilley, C. E. (1962). Origin of basalt magmas: an experimental study of natural and synthetic rock systems. *Journal of Petrology* **3**, 342–532.

Zhang, J. & Herzberg, C. (1994). Melting experiments on anhydrous peridotite KLB-1 from 5·0 to 22·5 GPa. *Journal of Geophysical Research* **99**, 17729–17742.